Research Letter DOI: 10.15541/jim20250076

A Rectifier Bridge Circuit Based on Metal-semiconductor-metal Fin Tunneling Diode for High-frequency Application

DENG Hengyang[1], QIN Cuijie[1], HAO Shenglan[1], FENG Guangdi[1,2], ZHU Qiuxiang[1], TIAN Bobo[1,2], CHU Junhao[1], DUAN Chungang[1,3]

(1. Shanghai Center of Brain-inspired Intelligent Materials and Devices, Key Laboratory of Polar Materials and Devices (MOE), Department of Electronics, East China Normal University, Shanghai 200241, China; 2. Chongqing Key Laboratory of Precision Optics, Chongqing Institute of East China Normal University, Chongqing 401120, China; 3. Collaborative Innovation Center of Extreme Optics, Shanxi University, Taiyuan 030006, China)

Abstract: Tunneling diodes hold significant promise for future rectification in the terahertz (THz) and visible light spectra, thanks to their femtosecond-scale transit-time tunneling capabilities. In this work, TiN/ZnO/Pt fin tunneling diodes (FTDs) with tunneling distances of 10 and 5 nm are fabricated, which demonstrate remarkable characteristics, including ultrahigh asymmetry (1.6×10^4 for 10 nm device and 1.6×10^3 for 5 nm device), high responsivity (25.3 V^{-1} for 10 nm device and 28.3 V^{-1} for 5 nm device) at zero bias, surpassing the thermal voltage limit of conventional Schottky diodes, and low turn-on voltage (V_{on}) of approximately 100 mV for both devices, making them ideal for power conversion applications. Using technology computer-aided design (TCAD) simulations, the observed asymmetry in electronic transport is attributed to the transition between Fowler-Nordheim tunneling (FNT) and trap-assisted tunneling (TAT) under different biasing conditions, as illustrated by the corresponding energy band profiles. Furthermore, by integrating the FTDs, a rectifier bridge circuit is designed and exhibits full-wave rectification behavior, validated through SPICE simulations for THz-band operations. This advancement offers a highly efficient solution for THz-band energy conversion and effective detection applications.

Key words: fin tunneling diode; TCAD simulation; rectifier bridge; SPICE simulation

Tunneling diodes play an indispensable role in a myriad of applications, such as energy harvesting[1-3], detectors[4-7], and wireless power transmission[8]. Their effectiveness stems from an ultrafast, quantum-based electron transport mechanism, characterized by a typical tunneling time on the order of femtoseconds[9]. The metal/insulator/metal (MIM) junctions, where a particularly thin insulator (less than 10 nm) is sandwiched between two distinct metals, form the core structure of these simple yet highly effective tunneling diodes. The rectification performance of a tunneling diode, derived from its current-voltage (*I*-*V*) curve, is characterized by the three key figures of merit (FOMs)[6, 10-15]: asymmetry (*i. e.*, rectification ratio), nonlinearity and responsivity, as shown in formulas (1)–(3). Asymmetry, the ratio of forward (I_F) to reverse (I_R) current at a given bias, reflects a diode's rectification capacity. Nonlinearity describes the sharpness of the diode's V_{on}, with higher nonlinearity enabling greater current density at lower voltages. Responsivity is defined as the direct current (DC) power output generated per unit of alternating current (AC) power input, reflecting the diode's nonlinearity. High responsivity is crucial for efficient small-signal rectification. Low V_{on}, high asymmetry and responsivity are essential for energy harvesting rectification[5, 16].

Received date: 2025-02-22; **Revised date:** 2025-03-14; **Published online:** 2025-05-09
Foundation item: National Key Research and Development Program of China (2024YFA1410700, 2021YFA1200700); National Natural Science Foundation of China (62474065, T2222025, 62174053); Natural Science Foundation of Chongqing (CSTB2024NSCQ-JQX0005); Shanghai Science and Technology Innovation Action Plan (24QA2702300, 24YF2710400); National Postdoctoral Program (GZB20240225); Fundamental Research Funds for the Central Universities
Biography: DENG Hengyang (1999–), male, Master candidate. E-mail: 51254700083@stu.ecnu.edu.cn
邓恒杨(1999–), 男, 硕士研究生. E-mail: 51254700083@stu.ecnu.edu.cn
Corresponding author: ZHU Qiuxiang, associate professor. E-mail: qxzhu@clpm.ecnu.edu.cn;
TIAN Bobo, professor. E-mail: bbtian@ee.ecnu.edu.cn
朱秋香, 副教授. E-mail: qxzhu@clpm.ecnu.edu.cn; 田博博, 教授. E-mail: bbtian@ee.ecnu.edu.cn

Asymmetry $$f_{\mathrm{Asy}} = \left| I_{\mathrm{F}} / I_{\mathrm{R}} \right| \quad (1)$$

Nonlinearity $$f_{\mathrm{NL}} = \frac{\mathrm{d}I}{\mathrm{d}V} \bigg/ \frac{I}{V} \quad (2)$$

Responsivity $$f_{\mathrm{Res}} = \frac{\mathrm{d}^2 I}{\mathrm{d}V^2} \bigg/ \frac{2\mathrm{d}I}{\mathrm{d}V} \quad (3)$$

Extensive research works have focused on enhancing rectification properties of MIM diodes through various methods, such as electrode or insulator material selection and structural design[5, 12, 17-18]. The conventional approach to achieving high asymmetry in MIM structures involves utilizing metal electrodes with dissimilar work functions and tuning the insulator layer[14]. Notably, Periasamy *et al.*[19] fabricated devices featuring the same M_1/I (Nb/Nb_2O_5) bilayer but varying M_2 bent wires to assess how the work function difference ($\Delta\varphi$) between electrodes impacts device performance. They found that asymmetry increased sharply for $\Delta\varphi$ exceeding k_BT, while nonlinearity exhibited a non-monotonic increase with $\Delta\varphi$[19]. Their hypothesis for optimizing MIM rectifier suggested that the electron affinity of the insulator should closely match the work function of one of the metals to achieve a low barrier height, thereby maximizing asymmetry and nonlinearity while minimizing the V_{on}[20]. The simulation work by Mistry *et al.*[21] also demonstrated that adjusting the electron affinity of insulator in MIM diode could reduce resistance and increase operating frequency, all while maintaining FOMs. However, performance of MIM tunneling diodes utilizing material selection method was restricted by the limited work function range of practical electrode materials, as well as a choice of the single insulator. Defect engineering offers an alternative approach. For instance, Mistry *et al.*[14, 21] found that $Pt/Al_2O_3/Al$ tunneling diodes fabricated *via* atmospheric pressure chemical vapor deposition exhibited Poole–Frenkel conduction at low biases and FNT at high biases due to hydroxyl group-induced electron traps. Additionally, these diodes have lower effective barrier height at the electrode/insulator interface compared to those fabricated *via* conventional methods, leading to reduced V_{on}, lower zero-bias resistance, and improved asymmetry[14, 22]. Holden *et al.*[16] introduced Ni impurities in $TiN/Al_2O_3/Al$ MIM diodes, strategically positioning defects near the Al electrode to reverse and enhance asymmetry. In addition, geometrical asymmetry is another appealing strategy[23-24]. Liu *et al.*[24] demonstrated that in PtNPs (Pt nanoparticles)/TiO_2/Pt MIM diodes, where nanoparticles concentrated electron density at the PtNPs side, the effective width of the tunneling barrier decreased under forward bias, resulting in a simultaneous increase in both current density and asymmetry compared to MIM diodes without nanoparticles. Despite advancements, MIM diodes face limitations in resistance and V_{on}, with responsivity being difficult to surpass the theoretical limit of 19.4 V^{-1} for Schottky diodes, which is defined by the inverse of the thermal voltage ($V_T = (q/2k_BT)$)[12]. Multi-insulator diodes (MIIM) can address high resistance and enhance FOMs by reducing the effective tunneling distance through stepped tunneling (ST) or resonant tunneling (RT)[4-5, 11-14, 16, 25-26]. Recently, Alshehri *et al.*[27] fabricated 414 ZnO/Al_2O_3 diodes to optimize film thickness, achieving a resistivity of ~4×10^3 Ω·cm, an asymmetry of 227, and a zero-bias responsivity of 12 V^{-1}. Nevertheless, MIIM fabrication remains challenging due to layer compatibility. It is worth mentioning that FTDs with a TiN/ZnO/Pt metal/semiconductor/metal (MSM) structure offer superior rectification, achieving an asymmetry of more than 10^4 by replacing the insulator with a semiconductor layer of sub-10 nm tunneling distance, which effectively narrows Schottky barriers and improves electron tunneling[28-29]. Further in-depth studies are required to fully understand the conduction mechanisms, optimize rectification performance, and evaluate the integration potential of FTDs for high-frequency rectification applications.

Here, by employing Pt and TiN as high- and low-work function metals, an asymmetric barrier configuration in TiN/ZnO/Pt FTDs comparable to MIIM structure was created. FTDs with tunneling distances of 10 and 5 nm were prepared. This design achieves excellent rectification, including ultrahigh asymmetry exceeding 10^4 for FTD (10 nm), high responsivity of 28.3 V^{-1} at zero bias for FTD (5 nm) and extremely low V_{on} of 100 mV for two FTDs, suitable for high-frequency rectification and power conversion. TCAD simulations were utilized to unveil the tunneling mechanism under positive/negative bias voltage. A full-wave rectifier bridge circuit with FTDs shows good rectification of sine wave signals. SPICE simulations further verified feasibility of FTDs for future high-frequency applications.

1 Experimental

The line array of TiN/ZnO/Pt FTDs was fabricated, as shown in Fig. 1. The upper left inset shows the structure of the device, with TiN layer and Pt layer, separated by 10 nm Al_2O_3 films, serving as the bottom and top electrodes, respectively. ZnO layer, as a common semiconductor material[30-32], is then deposited with a thickness of ~20 nm along the side of $TiN/Al_2O_3/Pt$ stack, forming the TiN/ZnO/Pt FTDs. The tunneling distance is determined by the thickness of the Al_2O_3 layer, which is 10 nm in this case. The optical image of an individual device, captured from the top view, is displayed in the upper right inset. See our previous work for the detailed preparation process[29].

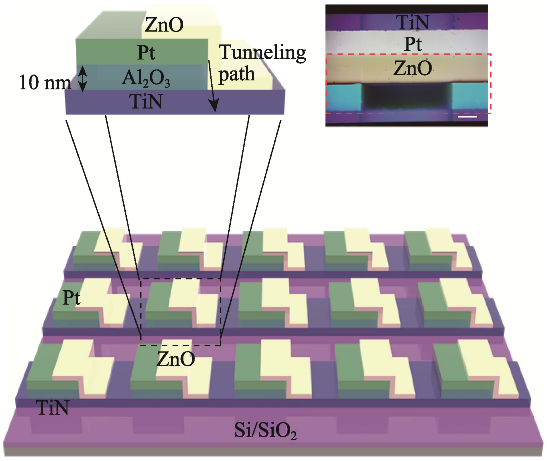

Fig. 1　Schematic diagram of line array constituted by TiN/ZnO/Pt FTDs fabricated on a Si/SiO$_2$ substrate, along with cross-sectional view of a single device

Upper right inset shows an optical image of an individual device from the top view (scale: 100 μm)

In this study, the full-wave rectifier bridge circuit based on TiN/ZnO/Pt FTDs is fabricated on a Si/SiO$_2$ substrate. Fabrication process of the rectifier bridge is shown in Fig. 2. The electronic transport properties of Pt/ZnO/TiN junctions FTDs are measured using a semiconductor parameter analyzer (Keithley 4200A-SCS). A sinusoidal input signal is generated by Agilent 33552A function generator, and the output waveform is captured using SIGLENT SDS1202X oscilloscope.

2　Results and discussion

2.1　Electrical characteristics and energy band alignments of TiN/ZnO/Pt FTDs

The energy band diagram alignments for TiN/ZnO/Pt after contact are depicted in Fig. 3(a), highlighting an asymmetric barrier that functions similarly to the interface barrier step in an MIIM structure. The work functions of Pt, TiN and ZnO are 5.02, 4.59, and 4.23 eV, respectively[29]. Given the heavy n-type doping of ZnO, its Fermi energy level is positioned near the bottom of the conduction band, with the electron affinity of ZnO approximately considered to be 4.23 eV. Upon contact between the electrodes and ZnO, the electrons in the semiconductor flow towards the metal, making the metal surface negatively charged and the semiconductor

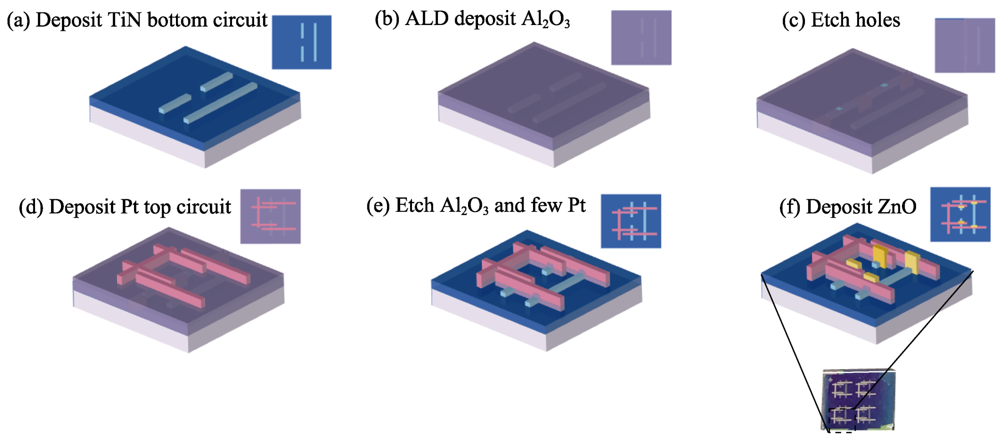

Fig. 2　Fabrication process of the rectifier bridge

(a) Deposit TiN bottom circuit; (b) ALD (Atomic layer deposition) deposit Al$_2$O$_3$; (c) Etch holes; (d) Deposit Pt top circuit; (e) Etch Al$_2$O$_3$ and few Pt; (f) Deposit ZnO

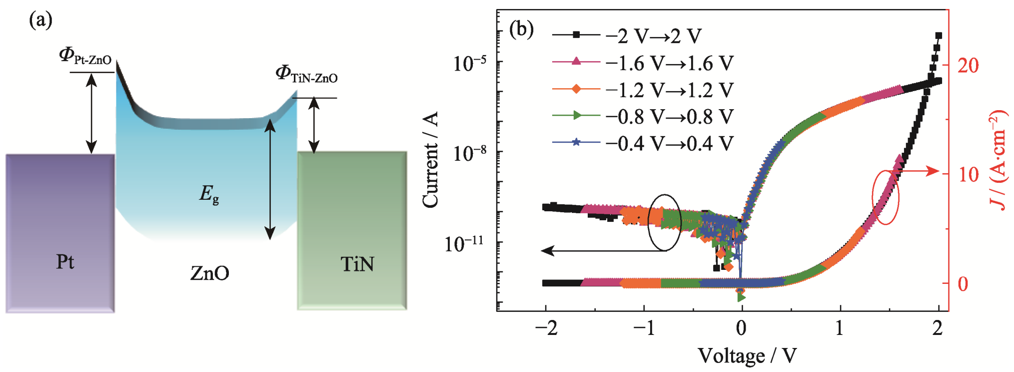

Fig. 3　Energy band alignments and electrical characteristics

(a) Energy band alignments of ZnO and electrodes (Pt and TiN) after contact; (b) *I-V* and *J-V* characteristics of the TiN/ZnO/Pt FTD device across various bias voltage ranges, where the bias is applied to the bottom electrode (TiN) and the top electrode (Pt) remains grounded surface positively charged, resulting in the alignment of their Fermi levels. In equilibrium, Schottky barriers are formed, with values calculated as 0.79 eV for Pt/ZnO and 0.36 eV for TiN/ZnO. Fig. 3(b) presents the *I-V* and *J-V* characteristics of the TiN/ZnO/Pt FTD device across various bias voltage ranges, where the bias is applied to the bottom electrode (TiN) and the top electrode (Pt) remains grounded. The measurements were conducted from –2 V to 2 V in increments of 0.02 V. The device exhibits excellent rectification performance, achieving an asymmetry of 1.07×10^3 at ±0.5 V with an on-state current density of 0.35 A/cm^2, and a maximum asymmetry of 1.61×10^4 at ±2 V with an on-state current of 22.6 A/cm^2.

2.2 Analysis of rectification mechanism

The conductive mechanism analysis is illustrated in Fig. 4. The energy band alignments under positive bias are illustrated in Fig. 4(a). When a positive bias is applied to the bottom TiN electrode, the Fermi level of TiN drops. As a result, electrons pass through the extremely skewed triangular barrier, which is narrower compared to that of conventional MIM diodes. The tunneling occurs from the Pt electrode to the TiN electrode *via* FNT[33], leading to a considerable current. The relationship between the FNT current *I* and the applied bias *V* is expressed as follows[10, 34-37]:

$$I(V)=\frac{Aq^3m_0V^2}{8\pi h\varphi_B d^2m^*}\exp\left[\frac{-8\pi\sqrt{2m^*}\Phi_B^{3/2}d}{3hqV}\right] \quad (4)$$

where A, Φ_B, q, m_0, m^*, d and h represent the effective contact area, barrier height, electron charge, free electron mass, effective electron mass ($0.1m_0$)[38], barrier width and Planck's constant, respectively. A highly linear relationship (R^2=0.999) of $\ln(I/V^2)$ *vs.* V^{-1} under high electric field in Fig. 4(b) indicates that the electronic property is well-fitted by the FNT model at positive voltage. $\Phi_{Pt\text{-}ZnO}$ extracted from the slope of the fitting line is approximately 0.23 eV, consistent with the previous work[10, 29]. There exists a slight discrepancy between the fitting result and the calculated value. Compared to the triangular barrier formed at the interface between a metal and an insulating material, the Schottky barrier created by the contact between a metal and semiconductor ZnO is much narrower[29]. This narrower width may lead to a reduction in the effective barrier height due to the influence of the image force and the quantum tunneling effect[39].

In Fig. 4(c), with a negative bias applied to the bottom TiN electrode, the electrons tunnel from TiN into Pt electrode. Direct tunneling (DT)[37], which involves one-step tunneling process, has been previously reported as the primary transport mechanism[29]. However, the DT model shows poor fitting under low-field conditions. Moreover, it should be noted that defects, such as oxygen vacancies, often occur during the deposition of ZnO semiconductors, which could facilitate assisted tunneling[10, 16]. Most of the electrons from TiN are firstly captured by trap states and subsequently emitted into the

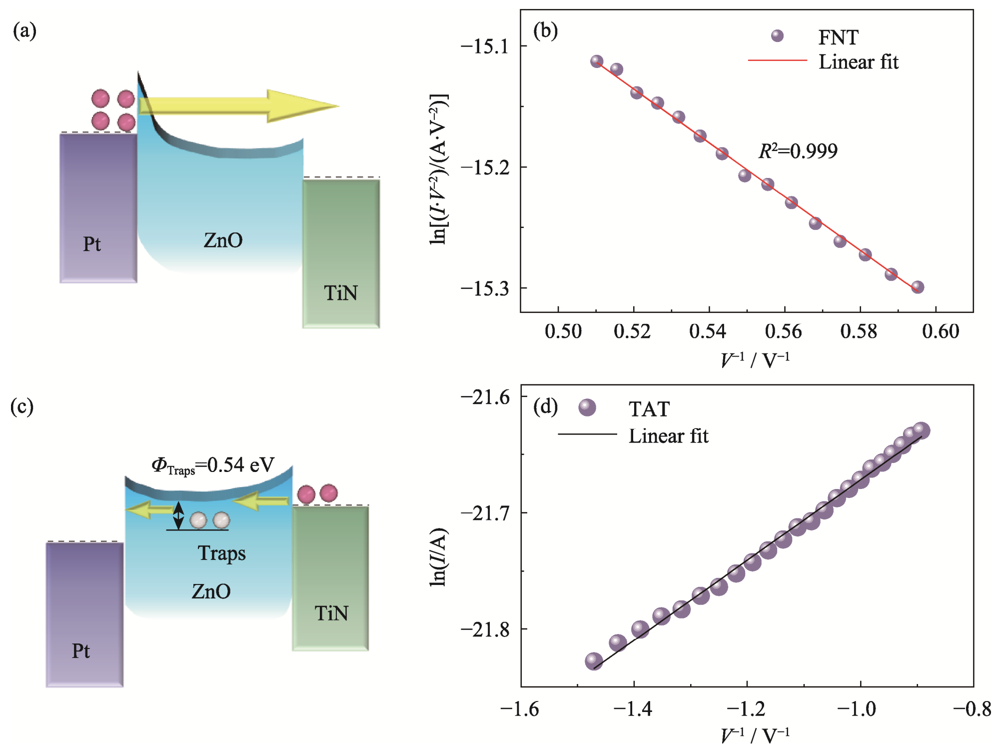

Fig. 4 Energy band alignments and fitting of tunneling mechanism of the FTD

(a) Energy band alignments of the FTD and (b) $\ln(I/V^2)$ *vs.* V^{-1} plots with FNT fitting under positive voltage; (c) Energy band alignments of the FTD and (d) $\ln I$ *vs.* V^{-1} plots with TAT fitting under negative voltage

Pt electrode, a process known as TAT[40]. The relationship between the current I and bias voltage V of TAT is expressed as follows[11, 17, 41]:

$$I(V) = C \cdot \exp\left(-\frac{8\pi\sqrt{2qm^*}\Phi_B^{3/2}}{3hV}\right) \quad (5)$$

where C is a constant. The linear fit of ln$I$ and V^{-1}, shown in Fig. 4(d), suggests that TAT dominates the electronic transport process. The currents under negative voltage remain low due to the significantly broad barrier width shown in Fig. 4(c). According to the fitting of TAT model, the trap energy level of ZnO is about 0.54 eV below the conductive band of ZnO. The position of trap level is shown in Fig. 4(c), consistent with previous report[42].

2.3 Rectification characteristics with different tunneling distances of 10 and 5 nm for TiN/ZnO/Pt FTDs

In order to explore the influence of tunneling thickness on rectification performance, TiN/ZnO/Pt FTD with a tunneling distance of 5 nm (*i.e.*, the thickness of Al_2O_3 is 5 nm) is fabricated. Fig. 5(a) presents the I-V curves of two FTDs with different tunneling distances. The current of 5 nm device gradually increases under negative voltage. This is likely due to the extremely short tunneling distance and stronger electrical field, allowing electrons to pass through the barrier more easily. V_{on} is determined through linear extrapolation of the I-V characteristics at the point where the current rises sharply. Based on energy band analysis, V_{on} is determined by the height of the TiN/ZnO barrier rather than the thickness of ZnO. As extracted from Fig. 5(b), V_{on} of two FTDs reaches an incredibly low value of 100 mV, promising greatly effective high-frequency rectification and power conversion. The current increases sharply by two orders of magnitude from 10^{-11} A at 100 mV to ~10^{-9} A at 200 mV. Figs. 5(c, d) present the rectification performance (resistivity, responsivity, asymmetry and nonlinearity) of the TiN/ZnO/Pt FTDs, as obtained using a 7-point Savitzky-Golay smoothing method[15]. For FTD (10 nm), asymmetry reaches a substantial value of 1.6×10^4 at ±2 V, and the zero-bias responsivity is impressively 25.3 V^{-1}, surpassing the responsivity limit of Schottky diodes (19.4 V^{-1}). Noticeably, the asymmetry remains significant for FTD (5 nm), reaching approximately 1.6×10^3 at ±1 V. It is worth mentioning that the device exhibits a zero-bias responsivity as high as 28.3 V^{-1} compared to FTD (10 nm). Moreover, the sandwiched TiN/ZnO/Pt tunneling diode was prepared and measured (not shown here), which shows low rectification performance. When compared with other tunneling diodes, as illustrated in Table 1, TiN/ZnO/Pt FTDs stand out for their excellent asymmetry, V_{on} and responsivity.

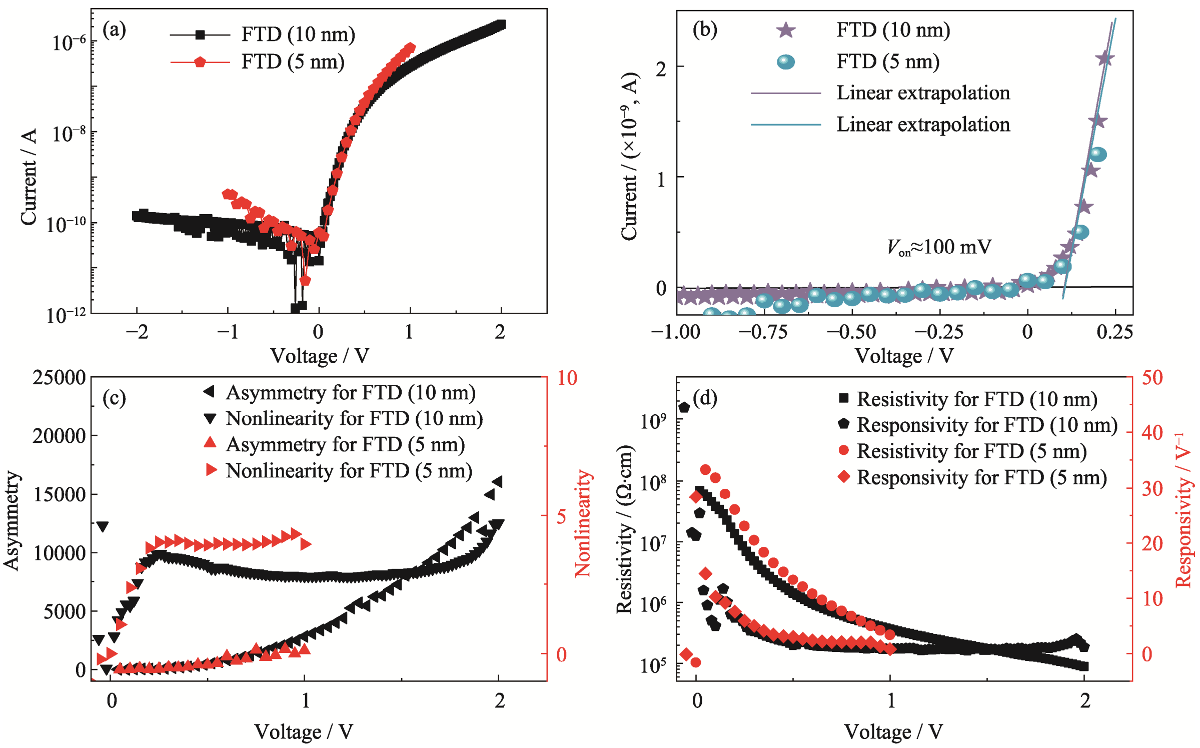

Fig. 5　Rectification performance of FTD (10 nm) and FTD (5 nm)

(a) I-V characteristics from experiments of FTD (10 nm) and FTD (5 nm); (b) I-V characteristics of FTD (10 nm) and FTD (5 nm) on a linear scale with V_{on} values being obtained by linear extrapolation; (c) Asymmetry and nonlinearity and (d) responsivity and resistivity of the TiN/ZnO/Pt FTD (10 nm) and FTD (5 nm)

The well-fitted curves in Figs. 6(a, b) also demonstrate that the conduction mechanism is dominated by FNT under high positive bias and TAT under negative bias in 5 nm device. To further explore the electronic transport mechanism of TiN/ZnO/Pt FTD (10 nm) and FTD (5 nm), TCAD simulations under positive/negative voltage are performed, with detailed simulation methodology provided next. The simulations reveal a transition between FNT under positive voltage and TAT under negative voltage, accounting for the high current rectification. The simulated *I-V* curves, shown in Fig. 7, align closely with experimental data.

The simulations of the ZnO-based MSM FTD are conducted using TCAD. The fabrication process begins with the deposition of a 10 nm Al_2O_3 layer onto a 60 nm-thick TiN electrode. Nextr, a 15 nm Pt top electrode is deposited, followed by the etching of excess Pt and Al_2O_3 on the right side. Finally, the semiconductor ZnO is deposited on the sidewall.

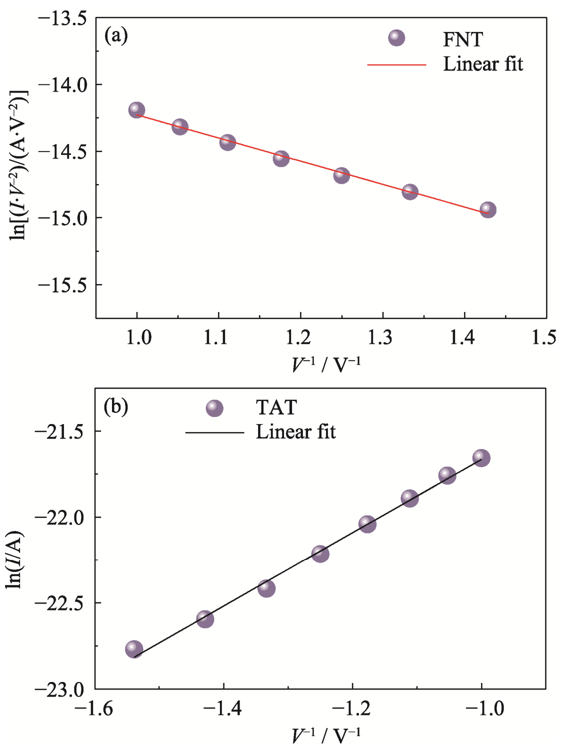

Fig. 6 Fitting of tunneling mechanism for FTD (5 nm)
(a) $\ln(I/V^2)$ *vs.* V^{-1} plots with FNT fitting under positive voltage; (b) $\ln I$ *vs.* V^{-1} plots with TAT fitting under negative voltage

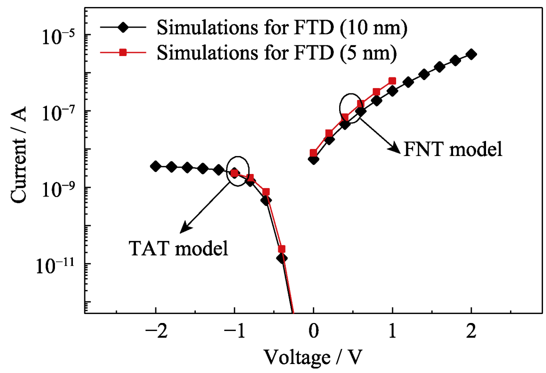

Fig. 7 *I-V* curves obtained from TCAD simulations for TiN/ZnO/Pt FTDs with tunneling distances of 10 and 5 nm, analyzed using the FNT model under positive bias and the TAT model under negative bias

In the simulation, n-type heavily doped ZnO with a carrier concentration of 10^{19} cm^{-3} is used. The work functions of Pt and TiN are 5.02 and 4.59 eV, respectively. The relative dielectric constants of ZnO and Al_2O_3 are 10 and 9, respectively. The electron affinity of ZnO is 4.23 eV, the bandgap width is 3.4 eV, the mobility model is OZGUR.N, the effective electron mass is $0.1m_0$[38], the defect energy level is 0.54 eV (measured from the ZnO conduction band), the defect density is 10^{15} cm^{-3}, and the degradation factor is 1. For a voltage range of 0–2 V, the FNORD and BBT.STD models are applied, while for –2–0 V, the MIM.ITAT.EL model is used. Considering the simulations and instrument accuracy, the current was processed below 10^{-14} A. In TiN/ZnO/Pt FTDs with different tunneling distances, only the thickness of the Al_2O_3 layer was modified, while all other physical quantities remained unchanged. The simulation results demonstrate a high degree of consistency with the experimental findings.

Table 1 Comparison of rectification performance among different tunneling diodes

Structure	f_{Asy}	V_{on}/V	f_{Res} (@0 V)/V^{-1}	Resistivity/(Ω·cm)
$Nb/Nb_2O_3/Pt$[19]	1500	0.15	10	8.3×10^8 (120 μm×120π μm)
Ni/NiO/ZnO/Cr[17]	16	0.25	<5	9.5×10^5 (20 μm×20 μm)
$Ti/TiO_2/Gr$[6]	320	~0.8	12	2.9×10^4 (140 $μm^2$)
Ti/ZnO/Pt[1]	<2	—	0.125	1.125×10^6 (0.09 mm^2)
$Co/Co_3O_4/TiO_2/Ti$[25]	2	—	2.2	5.8 (0.17 $μm^2$)
$Pt/Al_2O_3/Al$[10]	107	1.4	<5	8.3×10^{12} (100 $μm^2$)
$Pt/ZnO/Al_2O_3/Al$[27]	227	~0.5	13	3000–5000 (10 μm×10 μm)
$Cr/TiO_2/ZnO/Cr$[38]	5.6	—	0.28	1300 (10^4 $μm^2$)
FTD (10 nm) (This work)	1.6×10^4	0.1	25.3	8.8×10^4 (0.02 μm×500 μm)
FTD (5 nm) (This work)	1.6×10^3	0.1	28.3	8.8×10^4 (0.02 μm×500 μm)

2.4 Experiment and SPICE simulations of full wave rectifier bridge for TiN/ZnO/Pt FTDs

Considering the excellent rectifier stability of the individual devices, a full-wave rectifier circuit based on the TiN/ZnO/Pt FTDs on a silicon chip is designed and fabricated. The schematic diagrams of the measurement circuit and the equivalent full-wave rectifier circuit are shown in Figs. 8(a, b), respectively. The full-wave rectifier bridge consists of four FTDs, with two input terminals VIN1 and VIN2, and two output terminals VOUT1 and VOUT2, as illustrated in Figs. 8(c, d). In the circuit configuration, the bottom electrode TiN of FTD1 (FTD3) is connected with the top electrode Pt of FTD2 (FTD4), with the Pt electrode of FTD2 (FTD4) serving as VIN1 (VIN2). The top electrode Pt of FTD1 and FTD3 is jointly connected as VOUT1, and the bottom electrode TiN of FTD2 and FTD4 is connected together to form VOUT2. A full-wave rectifier bridge converts both the positive and negative halves of the input waveform to a single polarity (positive or negative) at its output, as shown on the right side of Fig. 8(d). The full-wave rectifier is tested with sinusoidal waves of V_{pp}= 1.5 V at different frequencies (1, 2, and 5 Hz), and the normalized test results are shown in Figs. 8(e-g). Furthermore, high-frequency rectification characteristics were validated through SPICE simulations. According to the parameters of the tunneling diode, the ideal physical model of FTD was established, and Table 2 lists the parameters. In the circuit design, an AC voltage source, tunable in voltage and frequency, is used in place of the antenna. Both the AC-to-DC conversion and high-frequency performance are investigated and analyzed. As shown in Fig. 9, the rectifier circuit effectively converts the 1 V, 100 GHz AC input signal (simulating the signal received by the antenna) into a 0.52 V DC voltage output. The DC output voltage stabilizes within 100 ms, demonstrating robust AC-to-DC conversion with the proposed FTDs. The conversion efficiency of the full-wave rectifier is expressed as:

$$\eta = P_{out} / P_{in} = V_{DC} \times I_{DC} / (V_{RMS} \times I_{RMS}) \quad (6)$$

where η, P_{out}, P_{in}, V_{DC}, I_{DC}, V_{RMS} and I_{RMS} represent conversion efficiency, output power, input power, DC voltage, DC current, root mean square (RMS) voltage and RMS current. In the SPICE simulations, the input sinusoidal waveform peak at 1 V and the frequency is 100 GHz, V_{DC} after capacitor filtering is 0.52 V, V_{RMS}= $V_{peak}/\sqrt{2}$ =1/ $\sqrt{2}$ V, I_{DC}=V_{DC}/R_L, I_{RMS}=$I_{DC}\times\pi/2\sqrt{2}$ A, here, V_{peak} means peak voltage, R_L means load resistance, and the final theoretical conversion efficiency is calculated to be ~66%.

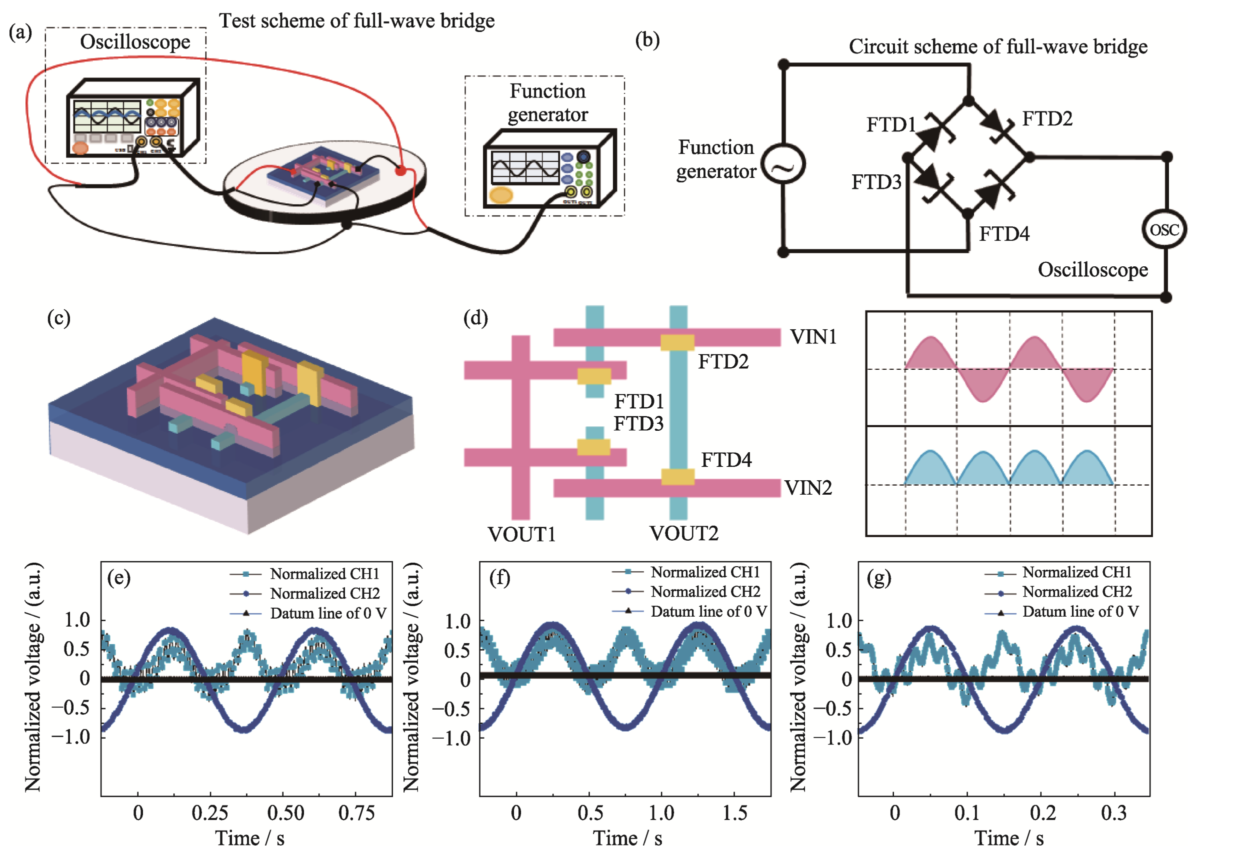

Fig. 8　Scheme and experiment for full-wave rectifier bridge

(a) Test scheme for full-wave rectifier bridge; (b) Circuit scheme for full-wave rectifier bridge; (c) Structure schematic of full-wave rectifier bridge; (d) Layout diagram of full wave rectifier circuit (left) and corresponding rectification result (right); (e-g) Normalized full-wave rectification results of full-wave rectifier based on the TiN/ZnO/Pt FTDs with V_{pp}=1.5 V at frequencies of 1 (e), 2 (f) and 5 Hz (g), respectively

Table 2 Parameters of the ideal physical model of FTD

Parameter	Description	Unit	Value
TOX	Thickness of tunneling layer	Å	100
IF	Forward Fowler-Nordheim current coefficient	A/V^2	5×10^{-16}
IR	Reverse Fowler-Nordheim current coefficient	A/V^2	1×10^{-16}
EF	Forward critical electric field	V/cm	2×10^{6}
ER	Reverse critical electric field	V/cm	2×10^{8}
L	Diode length	m	2×10^{-8}
W	Diode width	m	5×10^{-4}

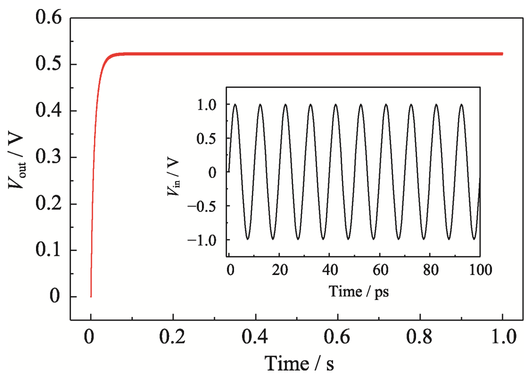

Fig. 9 SPICE simulations for the full-wave rectifier bridge based FTDs with a frequency of 100 GHz and V_{pp}=2 V

To enhance the conversion efficiency of the full-wave rectifier circuit in the experiment, several measures can be taken. Firstly, electron beam lithography (EBL) technology can be utilized to fabricate a tunnel diode with a smaller area. Secondly, selecting a capacitor with low equivalent series resistance (ESR) is essential to minimize energy dissipation. Lastly, impedance matching design is crucial, particularly in rectifying antenna applications. Properly designing the diode and antenna resistance can significantly improve rectification efficiency, which remains a pressing challenge in current rectifying antenna research. Additionally, it is important to ensure that the test environment is free from electromagnetic interference. Overall, these devices demonstrate great potential for THz-band rectification in energy conversion and detection technologies.

3 Conclusions

In summary, the rectification performance and mechanisms of TiN/ZnO/Pt FTDs with tunneling distances of 10 and 5 nm are comprehensively analyzed, and a full-wave rectifier bridge circuit based on these devices is proposed. Through TCAD simulations and energy band analysis, it is confirmed that the tunneling mechanisms in TiN/ZnO/Pt FTDs are dominated by FNT under positive bias and by TAT under negative bias. These FTDs exhibit great attributes, including high asymmetry, large responsivity, and extremely low V_{on}, and demonstrate outstanding rectification performance for sine wave signals.

References:

[1] KHAN A A, JAYASWAL G, GAHAFFAR F A, *et al*. Metal-insulator-metal diodes with sub-nanometre surface roughness for energy-harvesting applications. *Microelectron. Eng.*, 2017, **181:** 34.

[2] DRAGOMAN M, ALDRIGO M. Graphene rectenna for efficient energy harvesting at terahertz frequencies. *Appl. Phys. Lett.*, 2016, **109(11):** 113105.

[3] OLLER D, OSGOOD R, XU J, *et al*. Optical rectification in a reconfigurable resistive switching filament. *Appl. Phys. Lett.*, 2019, **115(4):** 043101.

[4] WEERAKKODY A, BELKADI A, MODDEL G. Nonstoichiometric nanolayered Ni/NiO/Al_2O_3/CrAu metal-insulator-metal infrared rectenna. *ACS Appl. Nano Mater.*, 2021, **4(3):** 2470.

[5] BELKADI A, WEERAKKODY A, MODDEL G. Demonstration of resonant tunneling effects in metal-double-insulator-metal (MI(2)M) diodes. *Nat. Commun.*, 2021, **12:** 2925.

[6] SHAYGAN M, WANG Z, ELSAYED M S, *et al*. High performance metal-insulator-graphene diodes for radio frequency power detection application. *Nanoscale*, 2017, **9(33):** 11944.

[7] SANCHEZ A, DAVIS C F, LIU K C, *et al*. The MOM tunneling diode: theoretical estimate of its performance at microwave and infrared frequencies. *J. Appl. Phys.*, 1978, **49(10):** 5270.

[8] NISHIDA Y, NISHIGAMI N, DIEBOLD S, *et al*. Terahertz coherent receiver using a single resonant tunnelling diode. *Sci. Rep.*, 2019, **9:** 18125.

[9] MITROVIC I Z, ALMALKI S, TEKIN S B, *et al*. Oxides for rectenna technology. *Materials*, 2021, **14(18):** 5218.

[10] ALSHEHRI A H, MISTRY K, NGUYEN V H, *et al*. Quantum-tunneling metal-insulator-metal diodes made by rapid atmospheric pressure chemical vapor deposition. *Adv. Funct. Mater.*, 2018, **29(7):** 1805533.

[11] ANDERSON E C, BOUGHER T L, COLA B A. High performance multiwall carbon nanotube-insulator-metal tunnel diode arrays for optical rectification. *Adv. Electron. Mater.*, 2018, **4(3):** 1700446.

[12] ALSHEHRI A H, SHAHIN A, MISTRY K, *et al*. Metal-insulator-insulator-metal diodes with responsivities greater than 30 A·W^{-1} based on nitrogen-doped TiO_x and AlO_x insulator layers. *Adv. Electron. Mater.*, 2021, **7(11):** 2100467.

[13] ALIMARDANI N, CONLEY J F. Enhancing metal-insulator-insulator-metal tunnel diodes *via* defect enhanced direct tunneling. *Appl. Phys. Lett.*, 2014, **105(8):** 082902.

[14] SHRIWASTAVA S, TRIPATHI C C. Metal-insulator-metal diodes: a potential high frequency rectifier for rectenna application. *J. Electron. Mater.*, 2019, **48(5):** 2635.

[15] ZHANG X, GRAJAL J, VAZQUEZ-ROY J L, *et al*. Two-dimensional MoS_2-enabled flexible rectenna for Wi-Fi-band wireless energy harvesting. *Nature*, 2019, **566(7744):** 368.

[16] HOLDEN K E K, QI Y, CONLEY J F. Precision defect engineering of metal/insulator/metal diodes using atomic layer deposition to localize Ni impurities in Al_2O_3 tunnel barriers. *J. Appl. Phys.*, 2021, **129(14):** 144502.

[17] SINGH A, RATNADURAI R, KUMAR R, *et al*. Fabrication and current-voltage characteristics of NiO_x/ZnO based MIIM tunnel diode. *Appl. Surf. Sci.*, 2015, **334:** 197.

[18] RATNADURAI R, KRISHNAN S, STEFANAKOS E, *et al*. Nanomanufacturability of thin film MIM diodes. *AIP Conference Proceedings*, 2010, **1313:** 403.

[19] PERIASAMY P, BERRY J J, DAMERON A A, *et al*. Fabrication and characterization of MIM diodes based on Nb/Nb_2O_5 *via* a rapid screening technique. *Adv. Mater.*, 2011, **23(27):** 3080.

[20] PERIASAMY P, GUTHREY H L, ABDULAGATOV A I, *et al*. Metal-insulator-metal diodes: role of the insulator layer on the rectification performance. *Adv. Mater.*, 2013, **25(9):** 1301.
[21] MISTRY K, YAVUZ M, MUSSELMAN K P. Simulated electron affinity tuning in metal-insulator-metal (MIM) diodes. *J. Appl. Phys.*, 2017, **121(18):** 184504.
[22] OZYIGIT D, ULLAH F, GULSARAN A, *et al*. Manufacturing of quantum-tunneling MIM nanodiodes *via* rapid atmospheric CVD in terahertz band. *Sci. Rep.*, 2023, **13(1):** 20733.
[23] WARD D R, HUSER F, PAULY F, *et al*. Optical rectification and field enhancement in a plasmonic nanogap. *Nat. Nanotechnol.*, 2010, **5(10):** 732.
[24] LIU Z, ABE S, SHIMIZU M, *et al*. Enhanced current density and asymmetry of metal-insulator-metal diodes based on self-assembly of Pt nanoparticles. *Appl. Phys. Lett.*, 2023, **122(9):** 093502.
[25] HERNER S B, WEERAKKODY A D, BELKADI A, *et al*. High performance MIIM diode based on cobalt oxide/titanium oxide. *Appl. Phys. Lett.*, 2017, **110(22):** 223901.
[26] MITROVIC I Z, WEERAKKODY A D, SEDGHI N, *et al*. Controlled modification of resonant tunneling in metal-insulator-insulator-metal structures. *Appl. Phys. Lett.*, 2018, **112(1):** 012902.
[27] ALSHEHRI A H, ASGARIMOGHADDAM H, DELUMEAU L V, *et al*. Combinatorial optimization of metal-insulator-insulator-metal (MIIM) diodes with thickness-gradient films *via* spatial atomic layer deposition. *Adv. Electron. Mater.*, 2024, **10(11):** 2400093.
[28] FENG G, ZHU Q, LIU X, *et al*. A ferroelectric fin diode for robust non-volatile memory. *Nat. Commun.*, 2024, **15:** 513.
[29] LIU X, FENG G, FENG X, *et al*. Ultrahigh rectification ratio in an asymmetric metal/semiconductor/metal nanoscale tunneling junction: implications for high-frequency rectifiers. *ACS Appl. Nano Mater.*, 2023, **6(4):** 2491.
[30] LIU H, ZHANG L, LEBEGUE S, *et al*. Morphology-electronic effects in ultra-model nanocatalysts under the CO oxidation reaction: the case of ZnO ultrathin films grown on Pt(111). *Nanoscale*, 2024, **16(43):** 20216.
[31] CHEN T, YU K, HU H, *et al*. Engineering electron transport layer with ionic liquid for high-performance quantum dot light-emitting diodes. *ACS Appl. Nano Mater.*, 2025, **8(9):** 4573.
[32] SHINDE P, HASE Y, DOIPHODE V, *et al*. Morphology-dependent ZnO/MoS_2 heterostructures for enhanced photoelectrochemical water splitting. *ACS Appl. Energ. Mater.*, 2025, **8(2):** 935.
[33] ALIMARDANI N, KING S W, FRENCH B L, *et al*. Investigation of the impact of insulator material on the performance of dissimilar electrode metal-insulator-metal diodes. *J. Appl. Phys.*, 2014, **116(2):** 024508.
[34] CONG X, ZHENG Y, HUANG F, *et al*. Efficiently band-tailored type-III van der Waals heterostructure for tunnel diodes and optoelectronic devices. *Nano Res.*, 2022, **15(9):** 8442.
[35] LEE G H, YU Y J, LEE C, *et al*. Electron tunneling through atomically flat and ultrathin hexagonal boron nitride. *Appl. Phys. Lett.*, 2011, **99(24):** 243114.
[36] MA Q, ANDERSEN T I, NAIR N L, *et al*. Tuning ultrafast electron thermalization pathways in a van der Waals heterostructure. *Nat. Phys.*, 2016, **12(5):** 455.
[37] VU Q A, LEE J H, NGUYEN V L, *et al*. Tuning carrier tunneling in van der waals heterostructures for ultrahigh detectivity. *Nano Lett.*, 2017, **17(1):** 453.
[38] TEKIN S B, ALMALKI S, FINCH H, *et al*. Electron affinity of metal oxide thin films of TiO_2, ZnO, and NiO and their applicability in 28.3 THz rectenna devices. *J. Appl. Phys.*, 2023, **134(8):** 084503.
[39] FOWLER R H, NORDHEIM L. Electron emission in intense electric fields. *Proc. Roy. Soc. A*, 1928, **119(791):** 173.
[40] YU S, GUAN X, WONG H S P. Conduction mechanism of $TiN/HfO_x/Pt$ resistive switching memory: a trap-assisted-tunneling model. *Appl. Phys. Lett.*, 2011, **99(6):** 063507.
[41] CHANG W J, HOUNG M P, WANG Y H. Electrical properties and modeling of ultrathin impurity-doped silicon dioxides. *J. Appl. Phys.*, 2001, **90(10):** 5171.
[42] TSIARAPAS C, GIRGINOUDI D, DIMITRIADIS E I, *et al*. Investigation on deep level defects in polycrystalline ZnO thin films. *J. Vac. Sci. Technol. B*, 2017, **35(3):** 031203.

基于金属-半导体-金属鳍式隧穿二极管的高频整流桥电路

邓恒杨[1], 秦翠洁[1], 郝胜兰[1], 冯光迪[1,2], 朱秋香[1],
田博博[1,2], 褚君浩[1], 段纯刚[1,3]

(1. 华东师范大学 电子科学系, 极化材料与器件教育部重点实验室, 上海类脑智能材料与器件研发中心, 上海 200241; 2. 华东师范大学重庆研究院 精密光学重庆市重点实验室, 重庆 401120; 3. 山西大学 山西省极端光学协同创新中心, 太原 030006)

摘 要: 隧穿二极管在太赫兹(THz)和可见光频谱的未来整流领域中具有显著的应用前景, 这得益于其拥有飞秒级的隧穿渡越时间。本研究制备了隧穿距离分别为 10 和 5 nm 的 TiN/ZnO/Pt 鳍式隧道二极管(Fin tunneling diodes, FTDs), 它们展现出优异的特性, 其中包括超高的不对称性(10 nm 器件为 1.6×10^4, 5 nm 器件为 1.6×10^3)、零偏压下的高响应度(10 nm 器件为 25.3 V^{-1}, 5 nm 器件为 28.3 V^{-1}), 均超越了传统肖特基二极管的热电压限制, 并且两个器件的开启电压(V_{on})都极低, 约为 100 mV, 这使得它们成为能量转换应用的理想选择。基于技术计算机辅助设计(Technology computer-aided design, TCAD)模拟, 所观测到的电子传输不对称性可归因于在不同偏置条件下福勒–诺德海姆隧穿(Fowler-Nordheim tunneling, FNT)和陷阱辅助隧穿(Trap-assisted tunneling, TAT)之间的转变, 这在相应的能带排列图中得以阐明。此外, 通过对 FTDs 进行集成, 设计了一种具有全波整流特性的整流桥电路, 其在太赫兹波段(0.1 THz)的整流性能通过 SPICE 电路仿真得到了验证。本研究为太赫兹能量转换和探测应用提供了一种高效的解决方案。

关 键 词: 鳍式隧穿二极管; TCAD 仿真; 整流桥; SPICE 仿真

中图分类号: TQ174 **文献标志码:** A **文章编号:** 1000-324X(2026)02-0253-09